Hybrid LES/URANS simulation of turbulent natural convection by BEM

CrossMark

P. Kocutar, L. Škerget, J. Ravnik *

Faculty of Mechanical Engineering, University of Maribor, Smetanova 17, SI-2000 Maribor, Slovenia

ARTICLE INFO

ABSTRACT

In this paper we have developed a hybrid LES/URANS turbulent model for a BEM based turbulent fluid flow solver. We employed the unified LES/URANS approach, where the interface between the LES and URANS regions is defined using a physical quantity, which dynamically changes during numerical simulation. The main characteristic of the unified hybrid model is that only one set of governing equations is used for fluid flow simulation in both the LES and URANS regions. Regions where turbulent kinetic energy is calculated by LES and URANS models are determined using a switching criterion. We used the Reynolds number based on turbulent kinetic energy and the Reynolds number based on total turbulent kinetic energy to establish the LES/URANS interface switching criterion. Depending on flow characteristics and with the use of switching criterion, we chose between sub-grid scale viscosity (SGS) and URANS effective viscosity. The SGS or URANS effective viscosity is used in the transport equation for turbulent kinetic energy and in governing equations for fluid flow. The developed numerical algorithm was tested by simulating turbulent natural convection within a square cavity. The hybrid turbulent model was implemented within a numerical algorithm based on the boundary element method, where single domain and sub-domain approaches are used. The governing equations are written in velocity–vorticity formulation. We used the false transient time scheme for the kinematics equation.

© 2015 Elsevier Ltd. All rights reserved.

1. Introduction

Turbulence occurs in fluid flows of high Reynolds numbers. It is present in the majority of fluid machines and devices, and is simulated during current engineering practise. Turbulence can be simulated by directly solving Navier–Stokes equations; this approach is called Direct Numerical Simulation, DNS. When using the DNS, we have to simulate flow phenomena that span the entire energy spectrum. As, at high Reynolds numbers, the Kolmogorov length scale is very small compared to the characteristic length scale of the flow, very dense meshes are required and thus high computational resources are demanded. As the DNS is very expensive from a computational point of view, it is currently being used mainly for research and to simulate benchmark cases. In the case of Large Eddy Simulation – LES – only those large eddies with the most energy are being simulated, while smaller eddies that cannot be described by the mesh are being modelled. Turbulent flow can also be simulated with Reynolds Averaged Navier Stokes equations using RANS and unsteady RANS (URANS) models. Despite some disadvantages, URANS models are more

widely used in turbulent fluid flow simulations and have become state-of-the-art in the CFD and engineering industry. URANS models demand reasonable computational resources.

URANS is successful when modelling thin, fully turbulent, locally attached boundary layers. In the near wall regions due to small turbulent structures LES requires very fine meshes. In the bulk flow, where the Kolmogorov length scale is larger, fine meshes are adequate. RANS only provides statistical information of the flow, therefore its simulation results lack important information, e.g. coherent structures and dominant frequencies. LES directly solves large-scale motions, therefore it also provides significant amounts of accurate information. RANS requires reasonable computational times, while the computational costs of LES are too high [7].

As both LES and URANS have certain advantages and disadvantages hybrid models have been introduced which combine these two models. The basic concept of LES/URANS hybrid turbulent models is to use LES within the bulk region, where LES provides better results than URANS, and to use URANS in the near wall regions, where the mesh is not dense enough to capture the flow structures required by LES. Although the concept of combining LES and URANS turbulent models is not new [25], there are also several open topics, e.g. coupling technique between LES and URANS regions, which quantity to use for the switching criterion, and which LES and URANS turbulent model is the more appropriate.

* Corresponding author. Tel.: +386 2 220 7745; fax: +386 2 220 7996.
E-mail addresses: primozkocutar@yahoo.com (P. Kocutar),
leopold.skerget@um.si (L. Škerget), jure.ravnik@um.si (J. Ravnik).

LES/URANS hybrid turbulent models can be divided into two approaches when selecting LES and URANS regions, segregated [16,4,8] and unified [9]. In regard to the segregated LES/URANS approach, the computational domain is divided before simulation into LES and URANS regions [28]. Using this approach, LES and URANS are solved separately.

Unified models are also known as global or universal models. The main characteristic of unified models is that they use the same set of governing equations for fluid flow simulation for both LES and URANS. Unified hybrid models are further divided according to a switching criterion between LES and URANS regions. This switching criterion can be defined as a hard interface, where the user defines it within geometry, or the interface is defined dynamically during the simulation according to the switching criterion. One of the first steps when combining LES and URANS turbulent models was turbulent flow simulation using Detached-Eddy Simulation DES [25]. The idea is to model the whole boundary layer where the attached eddies occur with the URANS models, and only separate region where the eddies are detached, with the LES model. The same concept was also used by Paik et al. [14]. For the DES model, both researchers used the Spalart–Almaras one-equation turbulent model for turbulent viscosity. Breuer et al. [2] used a unified LES/URANS hybrid turbulent model for simulation of turbulent channel flow and flow over a periodic hill. Davidson [3] used a partially averaged Navier–Stokes (PANS) model for a RANS/LES hybrid model. This hybrid model was tested in a channel flow and in a hump flow using embedded LES. Schmidt and Breuer [22] used a unified LES-URANS hybrid model utilizing a switching criterion based on turbulent kinetic energy. Simulation was performed on the 3-D diffuser flow and flow passed an airfoil. Hybrid models were also used for heat transfer problems. Kenjereš and Hanjalič [10] compared LES, T-RANS and the hybrid RANS/LES turbulent model for simulating thermal convection between two flat horizontal walls cooled from above and heated from below, and natural convection within a square cavity.

Our work is based on the use of BEM for fluid flow. Škerget and Rek [27] used the boundary-domain integral method for numerical solutions for incompressible fluid flow within a driven cavity. They used the velocity–vorticity formulations of governing equations for a simulation and false transient approach for the kinematic equation. Ravnik et al. [18] used LES for the simulation of natural convection within a rectangular enclosure. BEM has been used for the solution of the kinematic equation and is combined with FEM, which is employed for the kinetics equation. Ramšak and Škerget [17] studied thermal flow simulation using the multidomain boundary element method with mixed boundary elements and a subdomain technique. For turbulent flow simulation they used a two-equation k–ϵ turbulence model. Lupše et al. [12] studied turbulent flow using a velocity–vorticity form of governing equation and BEM. For the turbulent channel flow and backward facing step they used Spalart–Allmaras, Chien and Abe–Kondoh–Nagano turbulent models.

We have developed a hybrid LES/URANS turbulent model using BEM using a combination of single-domain and sub-domain approaches. We have used the LES/URANS hybrid model for non-stationary non-isothermal turbulent flow simulation. Using unified hybrid model, LES and URANS models are unified within transport equation for turbulent kinetic energy k and are being solved simultaneously. The LES and URANS regions are not defined before simulation but are dynamically defined during simulation itself. Therefore the user also avoids problems of unknown fluid flows. The numerical algorithm switches to URANS mode within the near wall region and to the LES mode in the bulk flow. Sub-grid viscosity is used in LES mode, while in URANS mode, URANS modelled viscosity is used.

A 2D benchmark simulation of natural convection in square cavity was used to test our BEM implementation of the hybrid model. We choose the benchmark simulation of natural convection in square cavity, because it is geometrically very simple and the boundary conditions are well defined and at the same time exhibits fully turbulent flow. Thus, we could focus our attention to the implementation of the hybrid model, such as determining of the LES/URANS region and switching criterion. Furthermore, the closed cavity case makes it easier to implement the hybrid model, as the model depends on the wall distance, which is well defined in this case. In the future, we plan to extend this work to other turbulent flows.

2. Governing equations

2.1. Velocity–vorticity formulation

The governing equations were written in the velocity–vorticity formulation. The fluid is considered to be incompressible fluid with constant molecular viscosity ν_m and constant heat diffusivity a_m. We employed the velocity–vorticity numerical scheme with a false transient time scheme for the kinematic equation.

Governing equations for kinematics and kinetics have to be filtered for LES simulation and averaged for URANS simulation. After averaging/filtering governing equations we introduce a turbulent viscosity. Within the URANS region it is calculated by the URANS model and in LES by the SGS model. In the unified hybrid turbulent model we solve only one set of governing equations. Due to simplicity, we use a further derivation of equation notation without filtered or averaged signs.

Filtered/time averaged governing equations for fluid flow can be defined with effective kinematic viscosity ν_{ef} and effective heat diffusivity a_{ef}. Effective kinematic viscosity is the sum of molecular and turbulent kinematic viscosity $\nu_{ef} = \nu_m + \nu_t$, effective heat diffusivity is the sum of molecular and turbulent heat diffusivity $a_{ef} = a_m + a_t$. The kinematics equation is the curl of the vorticity vector written as a pseudo-transient problem to allow an under relaxation approach, while the kinetics equation is the vorticity equation found by taking the curl of the momentum equation. The equation for kinematics for incompressible plane flow can be written in velocity–vorticity formulation as [12]

$$\frac{\partial^2 v_i}{\partial x_j \partial x_j} - \frac{1}{\alpha}\frac{\partial v_i}{\partial t} + e_{ijk}\frac{\partial \omega_k}{x_j} = 0, \tag{1}$$

where α is the under-relaxation parameter. The kinetics equation is written for the transport of vorticity, using the curl of the second extended form of the momentum conservation equation in primitive variables formulation [29]. It can be written as [21]

$$\frac{D\omega}{Dt} = \nu_{ef}\frac{\partial^2 \omega}{\partial x_j \partial x_j} + e_{ij}\frac{\partial(\beta_T g(T-T_0))}{\partial x_j} - e_{ij}\frac{\partial f_i^m}{\partial x_j}, \tag{2}$$

where T_0 is a reference temperature, β_T is a thermal volumetric expansion coefficient, g is a gravity force oriented in opposite y direction, ω is the z component of the vorticity vector and $\overline{f_i^m}$ is a term defined as

$$f_i^m = -e_{ij}\frac{\partial(\nu_{ef}\omega)}{\partial x_j} + 2\frac{\partial \nu_{ef}}{\partial x_j}\frac{\partial v_i}{\partial x_j} + 2e_{ij}\frac{\partial \nu_{ef}}{\partial x_j}\omega. \tag{3}$$

Since we simulate an incompressible fluid, therefore the only force acting on fluid in natural convection flow is buoyancy. The buoyancy effect is considered in the kinetic equation (2) by using Boussinesq's approximation. For solving non-isothermal turbulent flow, we used a linear relationship of turbulent thermal diffusivity a_t and turbulent viscosity ν_t, defined by the turbulent Prandtl number Pr_t as $a_t = \nu_t/Pr_t$.

The filtered/time averaged energy equation for temperature T can be written as [12]

$$\frac{\partial T}{\partial t} + \frac{\partial v_j T}{\partial x_j} = \frac{\partial}{\partial x_j}\left(\left(a_m + \frac{\nu_t}{Pr_t}\right)\frac{\partial T}{\partial x_j}\right), \tag{4}$$

where Pr_t is the turbulent Prandtl number.

The transport equation for turbulent kinetic energy k can be written as [2]

$$\frac{\partial k}{\partial t} + v_j\frac{\partial k}{\partial x_j} = \frac{\partial}{\partial x_j}\left[(\nu_m + \nu_t)\cdot\frac{\partial k}{\partial x_j}\right] + \underbrace{\nu_t\left(\frac{\partial v_i}{\partial x_j} + \frac{\partial v_j}{\partial x_i}\right)\frac{\partial v_i}{\partial x_j}}_{P} - D, \tag{5}$$

where P is the production part, D the dissipation part, and its sum is the source term I. ν_m is the molecular viscosity and ν_t is the turbulent viscosity.

The used one-equation hybrid turbulent model is based on the transport equation for turbulent kinetic energy (5). In the URANS region turbulent viscosity ν_t and dissipation part D computed with URANS model $\nu_{t,URANS}$ and D_{URANS} are used, and in the LES region turbulent viscosity and the dissipation part are computed with sub-grid scale model $\nu_{t,SGS}$ and D_{SGS} respectively.

3. Hybrid LES/URANS turbulent model

3.1. Turbulent model for LES

The LES subgrid scale viscosity is calculated as Pope [15]. Filter width Δ, dissipation part D_{sgs} and turbulent viscosity $\nu_{t,sgs}$ for the sub-grid model can be written as

$$\nu_{t,sgs} = C_\mu \cdot k^{1/2} \cdot \Delta, \quad D_{sgs} = C_d \cdot k^{3/2}/\Delta, \quad \Delta = (\Delta x \cdot \Delta y)^{1/2}. \tag{6}$$

where $C_d = 1.0$ and $C_\mu = 0.05$ [23].

3.2. Turbulent model for URANS

3.2.1. Rodi URANS model

We used the model developed by Rodi et al. [19]. This model is written using the following equations. Reynolds number defined with turbulent kinetic energy k can be written as $Re_k = k^{1/2} \cdot y/\nu$, where y is the normal distance from the wall. Turbulent viscosity can be written as $\nu_{t,URANS} = (\overline{v'^2})^{1/2} \cdot l_{\mu,\nu}$, characteristic length as $l_{\mu,\nu} = C_{l,\mu} \cdot y$, where $C_{l,\mu} = 0.33$ and the normal velocity fluctuations $\overline{v'^2}$ as $\overline{v'^2} = k \cdot (4.65 \cdot 10^{-5}Re_k^2 + 4.00 \cdot 10^{-4}Re_k)$. Empirical correlations for the dissipation part, D_{URANS}, which correlates velocity scale, length scale and time scale, can be written as $D_{URANS} = (\overline{v'^2})^{1/2} \cdot k/l_{D,\nu}$, and dissipation length as $l_{D,\nu} = 1.3 \cdot y/ (1+2.12\nu/y(\overline{v'^2})^{1/2})$. These equations are valid up to $Re_k \leq 60$.

3.2.2. High Reynolds number URANS model

Breuer et al. [2] used DNS simulation results from Moser et al. [13] for modification of the Rodi one-equation turbulent model presented in Rodi et al. [19]. It should be noted that this is not a high Reynolds turbulent model. The modified one-equation turbulent model can be written using the following equations. Normal wall velocity fluctuation $\overline{v'^2}$ as $\overline{v'^2} = k \cdot (3.55 \cdot 10^{-5}Re_k^2 + 6.50 \cdot 10^{-4} \cdot Re_k)$, where $C_{l,\mu} = 0.4$ and dissipation length $l_{D,\nu}$ as $l_{D,\nu} = 1.5 \cdot y/ (1+7.65\nu/y(\overline{v'^2})^{1/2})$.

3.3. LES/URANS switching criterion

In this section we describe the switching criterion for defining LES and URANS regions. The definition is based on physical quantity.

3.3.1. Switching using Reynolds number defined by turbulent kinetic energy k

In the numerical algorithm we used the Reynolds number, for the switching criterion defined by the turbulent kinetic energy k, noted as Re_k. Re_k can be defined by turbulent kinetic energy k, viscosity ν, and the normal distance from the wall y as

$$Re_k = \frac{k^{1/2} \cdot y}{\nu}. \tag{7}$$

In this way, switching criterion can be written as [2]

$$Re_k \leq C_{switch} \rightarrow \text{RANS mode},$$
$$Re_k > C_{switch} \rightarrow \text{LES mode}, \tag{8}$$

where the value of C_{switch} can be used up to 60.

3.3.2. Switching using Reynolds number defined by the total turbulent kinetic energy k_{tot}

The next switching criterion used in the hybrid model was the Reynolds number defined as total turbulent kinetic energy, Re_{tot}, which is defined similar to Re_k:

$$Re_{tot} = \frac{k_{tot} \cdot y}{\nu}. \tag{9}$$

where k_{tot} is defined as the sum of the modelled turbulent kinetic energy, which is being solved in the transport equation (5), and the resolved turbulent kinetic energy, k_{res}, which is calculated from the simulated velocity field. The total turbulent kinetic energy k_{tot} can be written as $k_{tot} = k + k_{res}$, where k_{res} is defined as $k_{res} = (v_i'v_i')_{res}/2$.

Part v_i' in the equation for k_{res} is the difference between the averaged and current velocities, and can be written as $v_i' = v_i - \overline{v_i}$. $\overline{v_i}$ is the averaged velocity, computed with averaging of resolved velocity field.

It can be seen from the equations for k_{res} and v_i', that for $(v_i'v_i')$ calculation of the averaged velocity field is required. Therefore Re_{tot} cannot be used as a switching criterion from the beginning of the simulation. To achieve successful simulation averaging should be done over time, when flow crosses domain at least once.

Re_{tot} as a switching criterion is used in a same way as Re_k [2]:

$$Re_{tot} \leq C_{switch} \rightarrow \text{RANS mode},$$
$$Re_{tot} > C_{switch} \rightarrow \text{LES mode}. \tag{10}$$

where the value of C_{switch} can be used up to 60.

3.4. Modification of turbulent viscosity within the URANS region

By using total kinetic energy k_{tot} instead of k in the equations for LES models 3–6 and in the equations for URANS models written in Sections 3.2.1 and 3.2.2, we also used total turbulent viscosity $\nu_{t,URANS}^{tot}$ instead of the primary used modelled turbulent viscosity $\nu_{t,URANS}$ [2]. Total turbulent viscosity $\nu_{t,URANS}^{tot}$ is the sum of the molecular and resolved turbulent kinetic energy: $\nu_{t,URANS}^{tot} = \nu_{t,URANS} + \nu_{t,URANS}^{res}$. The resolved turbulent kinetic energy does not only depend on current velocity field but also on the difference between the current and averaged velocity fields. When simulating steady-state flow, the resolved turbulent viscosity is zero, $\nu_{t,URANS}^{res} = 0$. Therefore, when simulating unsteady flow, the total turbulent viscosity $\nu_{t,URANS}^{tot}$ differs from the modelled turbulent viscosity $\nu_{t,URANS}$ within the range of unsteady character of the flow.

Too high values of $\nu_{t,URANS}^{tot}$ could occur due to unsteady character of total turbulent kinetic energy k_{tot}, therefore they could be modified. We modified $\nu_{t,URANS}$, because $\nu_{t,URANS}^{res}$ depends directly on flow.

The turbulent viscosity may be modified using a modification function f. Breuer et al. [2] defined f from results of DNS turbulent

channel flow as

$$f = \begin{cases} 0.3 \cdot Re_{tot}, & 0 \le Re_{tot} \le 1 \\ 0.3, & 1 < Re_{tot} \le 12 \\ 0.3 + (1.55 \cdot 10^{-4}(Re_{tot} - 12)^2), & 12 < Re_{tot} \le 60 \end{cases} \quad (11)$$

Turbulent viscosity $\nu_{t,URANS}$ can be modified with modification function f as

$$\nu_{t,URANS}^{mod} = \nu_{t,URANS}^{mod} \cdot (1 - f). \quad (12)$$

The above written modification function can only be used only for simulation, where Re_{tot} is being used as the switching criterion.

3.5. URANS islands in LES region

During turbulent flow simulation using the LES/URANS hybrid model, URANS islands occur within the LES region. For investigating whether URANS islands adversely effect simulation, we have prescribed a condition which partly prevents URANS islands within the LES region. When the flow is unsteady and the interface between LES and URANS regions changes dynamically, we have focused only on one single node. We prescribe the condition, if a single node were to be in the URANS mode and all other boundary nodes in the LES mode, that the node also stays in the LES mode. It was used for both switching criteria, Re_k and Re_{tot}.

3.6. Summary

In order to simplify the hybrid model's labelling we allocated numbers to each hybrid model and its configurations, as shown in Table 1.

The models differ in turbulent model for URANS, turbulent kinetic energy, switching criterion between LES and URANS regions and modification function for URANS region. In models 1, 3 and 4 the turbulent model presented by Rodi is used and in models 2, 5 and 6 the URANS model modified for higher Reynolds numbers is used. Models 1–2 are using turbulent kinetic energy k and models 3–6 are using total turbulent kinetic energy k_{tot}. In models 1–2 the Reynolds number Re_k is used for switching criterion and in models 3–4 the Reynolds number Re_{tot} is used. The modification function is used in models 4 and 6.

4. Numerical method

A numerical algorithm based on subdomain BEM with velocity–vorticity formulation of Navier–Stokes equations was used for fluid flow simulation [27]. We divide the effective viscosity ν_{ef} in BEM into the sum of constant and variable parts as

$$\nu_m + \nu_t = \nu_{ef} = \nu_0 + \tilde{\nu}. \quad (13)$$

We write thermal diffusivity in the same way:

$$a_m + a_t = a_{ef} = a_0 + \tilde{a}. \quad (14)$$

Table 1
LES/URANS hybrid turbulent models used in fluid flow simulations.

URANS model	Rodi	Higher Re	Rodi	Rodi	Higher Re	Higher Re
Turb. kinetic energy	k	k	k_{tot}	k_{tot}	k_{tot}	k_{tot}
Switching crit.	Re_k	Re_k	Re_{tot}	Re_{tot}	Re_{tot}	Re_{tot}
Modification funct. (3.4)	No	No	No	Yes	No	Yes
Hybrid model	1	2	3	4	5	6

4.1. Integral formulation of parabolic-diffusive fundamental solution

Kinetics equation (2) can be written as a non-homogeneous parabolic partial differential equation as

$$\nu_0 \frac{\partial^2 \omega}{\partial x_j \partial x_j} - \frac{\partial \omega}{\partial t} - \frac{\partial}{\partial x_j}\left(v_j \omega + \tilde{\nu} \frac{\partial \omega}{\partial x_j}\right) - \frac{1}{\rho_0} e_{ij} \frac{\partial \rho g_i}{\partial x_j} - e_{ij} \frac{\partial f_i^m}{\partial x_j} = 0 \quad (15)$$

where the last three parts represent pseudo-body forces. Parabolic-diffusion fundamental solution u^* is defined as

$$u^*(\xi, s; t_F, t) = \frac{1}{(4\pi\nu_0\tau)} e^{-r^2/\nu_0\tau}, \quad (16)$$

where (ξ, t_F) is a source point, (s, t) the reference point within a domain, τ the time step, and r the vector from source point ξ to reference point s. The approximation on equations (17) implies a constant representation of the field variable during one time step. Using parabolic-diffusion fundamental solution u^* and

$$U^* = \nu_0 \int_{t_{f-1}}^{t_f} u^* \, dt, \quad \frac{\partial U^*}{\partial n} = \nu_0 \int_{t_{f-1}}^{t_f} \frac{\partial u^*}{\partial n} \, dt, \quad \frac{\partial U^*}{\partial x_j} = \nu_0 \int_{t_{f-1}}^{t_f} \frac{\partial u^*}{\partial x_j} \, dt, \quad (17)$$

we can write Eq. (15) in integral form for planar flow

$$
\begin{aligned}
c(\xi)\omega(\xi, t_F) + \int_\Gamma \omega \frac{\partial U^*}{\partial n} d\Gamma = &\frac{1}{\nu_0} \int_\Gamma \left((\nu_0 + \tilde{\nu})\frac{\partial \omega}{\partial n} - \omega v_n\right) U^* \, d\Gamma \\
&+ \frac{1}{\nu_0} \int_\Omega \left(\omega v_j - \tilde{\nu}\frac{\partial \omega}{\partial x_j}\right)\frac{\partial U^*}{\partial x_i} \, d\Omega \\
&+ e_{ij}\frac{1}{\nu_0}\left(\int_\Gamma n_i g_j F U^* d\Gamma - g_j F \frac{\partial U^*}{\partial x_i} \, d\Omega\right) \\
&- e_{ij}\frac{1}{\nu_0}\left(\int_\Gamma f_i^m n_j U^* d\Gamma - \int_\Omega f_i^m \frac{\partial U^*}{\partial x_j} \, d\Omega\right) \\
&+ \int_\Omega \omega_{F-1} u_{F-1}^* \, d\Omega.
\end{aligned}
\quad (18)
$$

The same idea as used for the kinetics equation can be used for the kinematics equation. Kinematics equation (1) can be written in the same manner as Eq. (15). In regard to further simplification of the numerical algorithm, we choose the under-relaxation term of false transient time scheme α to be equal to the viscosity term ν_0, and can write

$$\nu_0 \frac{\partial^2 v_i}{\partial x_j \partial x_j} - \frac{\partial v_i}{\partial t} + \nu_0 e_{ij} \frac{\partial \omega}{\partial x_j} = 0. \quad (19)$$

By considering (17) and (19), we may write kinematic equation (1) in integral form as

$$
\begin{aligned}
c(\xi)v_i(\xi, t_F) + \int_\Gamma v_i \frac{\partial U^*}{\partial n} d\Gamma \\
= \int_\Gamma \left(\frac{\partial v_i}{\partial n} + \nu_0 e_{ij}\omega n_j\right) U^* \, d\Gamma - \int_\Omega \nu_0 e_{ij}\omega \frac{\partial U^*}{\partial x_j} \, d\Omega + \int_\Omega v_{F-1} u_{F-1}^* \, d\Omega.
\end{aligned}
\quad (20)
$$

Eq. (20) obtained for unknown domain velocity values can be written as

$$
\begin{aligned}
c(\xi)v_i(\xi, t_F) + \int_\Gamma v_i \frac{\partial U^*}{\partial n} d\Gamma \\
= \int_\Gamma \nu_0 e_{ij} v_j \frac{\partial U^*}{\partial t} \, d\Gamma - \int_\Omega \nu_0 e_{ij}\omega \frac{\partial U^*}{\partial x_j} \, d\Omega + \int_\Omega v_{F-1} u_{F-1}^* \, d\Omega,
\end{aligned}
\quad (21)
$$

where n stands for unit normal and t for unit tangent.

Kinematics equation (1) is used also to determine boundary vorticity value, using the approach proposed by [26]. Eq. (20) rewritten for the solution of unknown boundary vorticity values can be written in vector form as

$$c(\xi)\vec{n}(\xi) \times \vec{v}(\xi) + \vec{n}(\xi) \times \int_\Gamma (\vec{\nabla} U^* \cdot \vec{n}) \vec{v} \, d\Gamma$$

$$= \vec{n}(\xi) \times \int_{\Gamma} (\vec{\nabla} U^* \times \vec{n}) \times \vec{v} \, d\Gamma + \vec{n}(\xi) \times \int_{\Omega} (\vec{\omega} \times \vec{\nabla} U^*) \, d\Omega. \tag{22}$$

4.2. Discrete form

The governing equations for fluid flow have to be rewritten in discrete form. The domain is divided into C internal cells and E boundary elements: $\Gamma = \sum_{e=1}^{E} \Gamma_e$, $\Omega = \sum_{c=1}^{C} \Omega_c$.

In regard to the approximated numerical solutions of field functions (velocity, vorticity, temperature, turbulent kinetic energy, etc.), the boundary-domain transport equation has to be written in discrete form, for the sum of integrals over every boundary element E and computational cell C. For interpolation of field function over boundary element and computational cell, we used interpolation functions: Φ for boundary elements and ϕ for computational cells. In the presented study we used quadratic interpolation for function nodes and constant fluxes. In the discrete equation formulation we used the following integrals:

$$h_e^p = \int_{\Gamma_e} \Phi^p \frac{\partial U^*}{\partial n} \, d\Gamma, \quad g_e^p = \int_{\Gamma_e} \Phi^p U^* \, d\Gamma, \quad d_{c_j} = \int_{\Omega_e} \phi^p \frac{\partial U^*}{\partial x_j} \, d\Omega,$$

$$d_c^p = \int_{\Omega_e} \phi^p U^* \, d\Omega, \quad b_c^p = \int_{\Omega_e} \phi^p u_{F_1}^* \, d\Omega. \tag{23}$$

Index p refers to the number of nodes in each internal cell or boundary element, and index m labels the degree of time polynomial (ψ). The equation for kinematics (20) can be, by employing parabolic-diffusion fundamental solution u^* and time step F, written for planar flow as

$$c(\xi)v_i(\xi) + \sum_{e=1}^{E} \{h\}^T \{v_i\} = \sum_{e=1}^{E} \{g\}^T \left\{ \nu_0 e_{ij} v_j \frac{\partial U^*}{\partial t} \right\}^p$$
$$- \nu_0 e_{ij} \sum_{c=1}^{C} \{d_j\}^T \{\omega\}^p + \beta \sum_{c=1}^{C} \{b\}^T \{v_i\}_{F-1}^p, \tag{24}$$

where T stands for the transposition and brackets { } refers to the vectors of nodal values. Equation for kinetics (18) can be written as

$$c(\xi)\omega(\xi) + \sum_{e=1}^{E} \{h\}^T \{\omega\} = \frac{1}{\nu_0} \sum_{e=1}^{E} \{g\}^T \left\{ \nu_{ef} \frac{\partial \omega}{\partial n} - \omega v_n \right\}^p$$
$$+ \frac{1}{\nu_0} \sum_{c=1}^{C} \{d_i\}^T \left\{ \omega v_i - \tilde{\nu} \frac{\partial \omega}{\partial x_j} \right\}^p$$
$$- e_{ij} \frac{1}{\nu_0} \sum_{e=1}^{E} \{g\}^T \{f_i^m\} + e_{ij} \frac{1}{\nu_0} \sum_{c=1}^{C} \{d_i\}^T \{f_i^m\}$$
$$+ e_{ij} \frac{1}{\nu_0} \sum_{e=1}^{E} \{g\}^T \{n_i g_j F\}^p - e_{ij} \frac{1}{\nu_0} \sum_{c=1}^{C} \{d_i\}^T \{g_j F\}^p$$
$$+ \beta \sum_{c=1}^{C} \{b\}^T \omega_{F-1}^p. \tag{25}$$

Transport equation for turbulent kinetic energy k (5) can be written as

$$c(\xi)u(\xi, t_F) + \sum_{e=1}^{E} \{h\}^T \{u\}_F^p = \frac{1}{\nu_0} \sum_{e=1}^{E} \{g\}^T \left\{ (\nu_0 + \tilde{\nu}) \frac{\partial u}{\partial n} \right\}_F^p$$
$$- \frac{1}{\nu_0} \sum_{e=1}^{E} \{g\}^T \{uv_n\}_F^p + \frac{1}{\nu_0} \sum_{c=1}^{C} \{d_j\}^T \left\{ uv_j - \tilde{\nu} \frac{\partial u}{\partial x_j} \right\}_F^p$$
$$+ \frac{1}{\nu_0} \sum_{c=1}^{C} \{d\}^T \{I\}_F^p + \sum_{c=1}^{C} \{b\}^T \{u\}_{F-1}^p. \tag{26}$$

and energy equation (4) as

$$c(\xi)T(\xi, t_F) + \sum_{e=1}^{E} \{h\}^T \{u\}_F^p$$

$$= \frac{1}{a_0} \sum_{e=1}^{E} \{g\}^T \left\{ (a_0 + \tilde{\nu}) \frac{\partial T}{\partial n} \right\}_F^p$$
$$- \frac{1}{a_0} \sum_{e=1}^{E} \{g\}^T \{Tv_n\}_F^p + \frac{1}{a_0} \sum_{c=1}^{C} \{d_j\}^T \left\{ Tv_j - \tilde{\nu} \frac{\partial T}{\partial x_j} \right\}_F^p$$
$$+ \sum_{c=1}^{C} \{b\}^T \{T\}_{F-1}^p. \tag{27}$$

According to boundary conditions we have assembled a system of equations written in matrix notation. We employed the numerical solver [24] for solving the system of equations.

5. Numerical algorithm

The implementation of a hybrid model within a numerical algorithm is shown step by step below. SGS and URANS turbulent viscosity, dissipation part and interface (step 6.1) are computed within the outer-loop for effective viscosity (step 6). Computed turbulent values η_{ef} and D are further being used in the solver for turbulent kinetic energy k equation (step 6.4) and in next time-step (step 1) for governing equations for fluid flow (steps 3–5).

1. Time loop
2. Global iteration loop
3. Kinetics loop
   - 3.1 kinematics, solve boundary vorticity ω
   - 3.2 kinematics, solve internal velocity v
   - 3.3 check convergence ω, v, if error is greater than predefined convergence criterion ϵ_m go to (3.1)
4. kinetics, solve energy equation
5. kinetics, internal vorticity ω
6. outer loop for effective viscosity ν_{ef}
   - 6.1 inner iteration loop for effective viscosity ν_{ef}
   - 6.2 turbulence model, calculate turbulence viscosity and dissipation part for sub-grid model ν_{sgs}, D_{sgs}, Eqs. (6) and for URANS model ν_{URANS}, D_{URANS}, Sections 3.2.1 and 3.2.2, interface between LES and URANS region, Section 3.3, define D and ν for further time steps 6.5 and 1.
   - 6.3 inner iteration loop for turbulent kinetic energy k
   - 6.4 kinetics, solve turbulent kinetic energy equation k
   - 6.5 check convergence for k, if error is greater than ϵ_k go to 6.3
   - 6.6 check convergence for ν_{ef}, if error is greater than ϵ_t go to 6.2
   - 6.7 check convergence for ν_{ef}, if error is greater than ϵ_t go to 6.1
7. check convergence for ω, T, if error is greater than ϵ go to 2.
8. time loop, if simulation not finished go to 1.
9. end of computation, write results

The convergence criteria used in the numerical algorithm were $\epsilon_k = 10^{-4}$, $\epsilon = 5 \cdot 10^{-6}$, $\epsilon_t = 10^{-3}$, and $\epsilon_m = 10^{-4}$. We used under-relaxations of all equations using values between 0.1 and 0.3.

6. Simulation of natural convection flow within a square cavity

We tested our numerical algorithm by simulating an unsteady turbulent natural convection flow within a square cavity. One of the first authors who studied such flows was Davies [5]. He published results regarding the simulation of natural convection flow within a square cavity up to Rayleigh number $Ra = 10^6$, and proposed natural convection flow within the square cavity as a benchmark case for solving non-isothermal fluid problems. Further research was done by Lo et al. [11], who used the velocity–vorticity formulation of Navier–Stokes equations for

natural convection flow simulation up to $Ra = 10^6$. Sajjadi et al. [20] investigated natural convection flow within a square cavity employing Large Eddy Simulation and the Lattice Boltzmann method for Rayleigh numbers from $Ra = 10^6$ to $Ra = 10^9$. Natural convection flow within the square cavity is steady up to Rayleigh number $Ra = 10^7$. At $Ra = 10^8$ it becomes unsteady, but not yet turbulent, the flow is not chaotic. When the flow reaches Rayleigh number $Ra = 10^9$, the flow is unsteady, chaotic, and turbulent. The boundary conditions are defined in Fig. 1 (left): temperature $T_h = 0.5$ on the uniformly heated left wall, adiabatic boundary condition $q = 0$ on the upper and lower walls, temperature $T_c = -0.5$ on the uniformly cooled right wall, no slip velocity $\vec{v} = 0$ boundary conditions on all four walls, and gravity $\vec{g}$ in the opposite direction of coordinate y. The problem is defined by the Rayleigh number. The Rayleigh number and the Prandtl number, which is $Pr = 0.71$, can be defined as

$$Ra = \frac{g \cdot \beta \cdot \Delta T \cdot L^3}{\nu \cdot \alpha}, \quad Pr = \frac{\nu}{\alpha}. \tag{28}$$

We assumed that the medium in the cavity is air with the following fluid properties: kinematic viscosity $\nu = 17.6 \cdot 10^{-6}$ m^2/s, thermal volumetric expansion coefficients $\beta = 1/313.15$ K^{-1} and thermal conductivity $\lambda = 0.0265$ W/mK. The height and width of a cavity is $L = 0.5$ m. Physical temperature difference between the heated and cooled walls is $\Delta T = 111.4$ K at $Ra = 10^9$.

During simulation, we used computational mesh with 80×80 domain elements and 161×161 nodes. The mesh was compressed in the normal wall direction in both coordinates with the geometrical series having the ratio between the longest and shortest elements $R = 10$.

The results of simulating natural convection fluid flow are evaluated using the averaged Nusselt number. The Nusselt number measures the heat flux through a solid wall and can be defined as

$$Nu = \frac{1}{H} \int_0^H \frac{\partial T}{\partial x} dy. \tag{29}$$

7. Results

7.1. Laminar natural convection at $Ra = 10^3 - 10^8$

Before employing the LES/URANS hybrid model and choosing appropriate computational mesh, we validated our numerical algorithm on laminar simulations of natural convection flow for Rayleigh numbers from $Ra = 10^3$ to $Ra = 10^8$. Simulations up to $Ra = 10^7$ were steady and simulation with $Ra = 10^8$ unsteady. For numerical algorithm validation we used three different computational meshes: $40 \times 40R10$, $80 \times 80R10$, and $120 \times 120R10$; which meant 81×81, 161×161, and 241×241 nodes. Simulation results for the lower and middle Rayleigh numbers are shown in Table 2, and are compared with the results from other authors. Simulations with computational mesh $40 \times 40R10$ up to $Ra = 10^8$ provided comparable results as simulations using $80 \times 80R10$ and $120 \times 120R10$. Mesh $40 \times 40R10$ was too coarse for natural convection flow simulation at $Ra = 10^9$, high temperature gradients and a thin boundary layer can be seen in further results. It should been noticed that, for mesh $40 \times 40R10$, the simulations for $Ra = 10^7$ and $Ra = 10^8$ were unsteady, results in brackets ( ) in Table 2. We concluded from mesh analysis using DNS for low and middle Rayleigh numbers, that in further simulations mesh $80 \times 80R10$ would be used. It can be seen that the values of the Nusselt number are within the same range; therefore we concluded that a numerical algorithm is appropriate for further simulations using turbulent models.
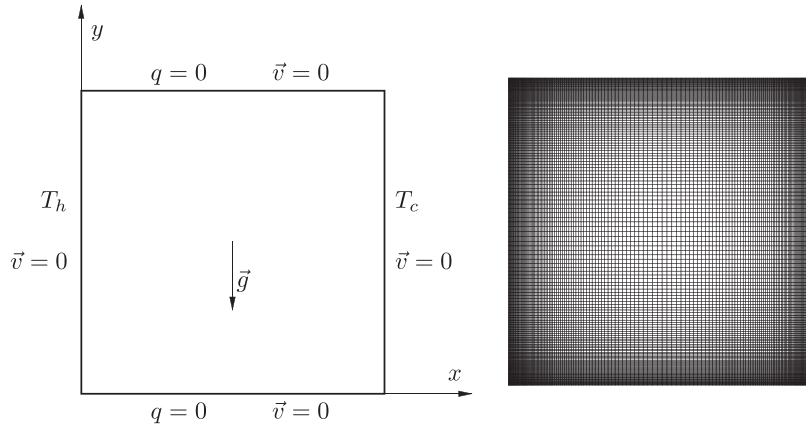
Fig. 1. Boundary conditions for test case simulation of natural convection flow within square cavity (left). Mesh used in simulation with 80×80 computational cells and ratio between longest and shortest elements $R = 10$ (right).

Table 2
Nusselt number for natural convection flow simulation using DNS for Rayleigh number from $Ra = 10^3$ to $Ra = 10^8$. Values in brackets ( ) display the averaged results for unsteady laminar simulation and the values in square brackets, the results when using turbulent models.

Ra	Barakos et al. [1]	Davies [5]	Dixit and Babu [6]	Lo et al. [11]	Sajjadi et al. [20]	Present 40×40	Present 80×80	Present 120×120
10^3	1.114	1.118		1.118		1.1178	1.1173	1.1174
10^4	2.245	2.243		2.224		2.2438	2.2434	2.2438
10^5	4.510	4.519		4.521		4.5207	4.5215	4.5217
10^6	8.806	8.8		8.823	8.7	8.8231	8.8222	8.8200
10^7		16.79			17.2	(16.518)	16.372	16.503
10^8	[32.3] (30.1)		(30.506)		[31.2]	(30.119)	(30.15)	(30.16)

Fig. 3 (left) shows the temperature profiles for Rayleigh numbers from $Ra = 10^3$ to $Ra = 10^8$ at height $y = L/2$ and length $x = L/2$. Fig. 2 shows the temperature field for $Ra = 10^7$ (left) and $Ra = 10^8$ (right). It can be seen from Fig. 2 that the temperature isolines are in the middle of the cavity almost parallel, and temperature stratification occurs. Natural convection flow up to Rayleigh number $Ra = 10^7$ is stationary, but at $Ra = 10^8$ flow becomes unsteady, but not yet chaotic and turbulent. We used DNS for simulations up to $Ra = 10^8$. The time-step used in the simulation at $Ra = 10^8$ was $\Delta t = 10^{-5}$.

7.2. Turbulent natural convection at $Ra = 10^9$

Simulations of turbulent natural convection flow were performed using 6 different hybrid LES/URANS turbulent models. Time step used in the simulation at $Ra = 10^9$ was $\Delta t = 5 \times 10^{-7}$. Time series for calculating the averaged Nusselt number was approximately 6000 time steps for hybrid models 1 and 2, approximately 11,000 for hybrid models 3 and 4, and approximately 8500 for hybrid models 5 and 6.

Fig. 4 shows temperature–vorticity phase portraits for $Ra = 10^9$ using computational mesh $80 \times 80R10$ and different hybrid models, 1–6. It can be seen that the nature of the flow is turbulent, unsteady, and chaotic. In natural convection flow, transition to turbulent flow occurs between $Ra = 10^8$ and 10^9. The unsteady and chaotic characteristics of natural convection flow can be seen in Fig. 6, that shows the temperature and the vorticity field for $Ra = 10^9$ using hybrid models 1 and 3. The main force acting on the fluid in the natural convection flow is buoyancy due to temperature difference and

gravity. As the vertical walls are being heated and cooled, fluid accelerates when passing by vertical walls. Although the flow is turbulent near the vertical walls, the majority of eddies are formed in the corners. In the figures it can also be seen that the boundary layer near the vertical walls is thin and the temperature gradients are high, therefore mesh should be compressed towards the walls. Fig. 3 (right) shows temperature profiles for Rayleigh number $Ra = 10^9$ at height $y = L/2$ and length $x = L/2$, using hybrid models from 1 to 6. The biggest difference between the temperature profiles for $Ra = 10^8$ and $Ra = 10^9$ is in the vertical profile in length $x = L/2$. Although the profiles for $Ra = 10^9$ show the same trend, it can be seen that the profile for hybrid model 1 deviates slightly from those profiles using other hybrid models. Fig. 5 shows the temperature time series power spectra at points A (0.05061, 0.05061) and B (0.09857, 0.09857) for different hybrid models. A power spectrum was calculated using fast Fourier Transform. Power spectra show the frequencies of eddies forming oscillations and consequently the presence of eddies of the different sizes. It can be seen that the widest frequency band occurs using models 1 and 2; the presence of smaller and larger eddies is more uniform. We noticed the power decay with the frequency, which was also noticed by other researchers [15].

When comparing the temperature and vorticity field in Fig. 6 with the LES/URANS regions in Fig. 8, we can see that URANS was used in near walls regions where attached eddies occurred and LES was used where detached eddies occurred. It can be seen from the time trace of the Nusselt number (Fig. 7) and the averaged Nusselt number values (Table 3) that the modification function has an effect on the flow. As turbulent viscosity ν_t and heat conductivity are in linear connection with the turbulent Prandtl number Pr_t, no clear trend could be done,
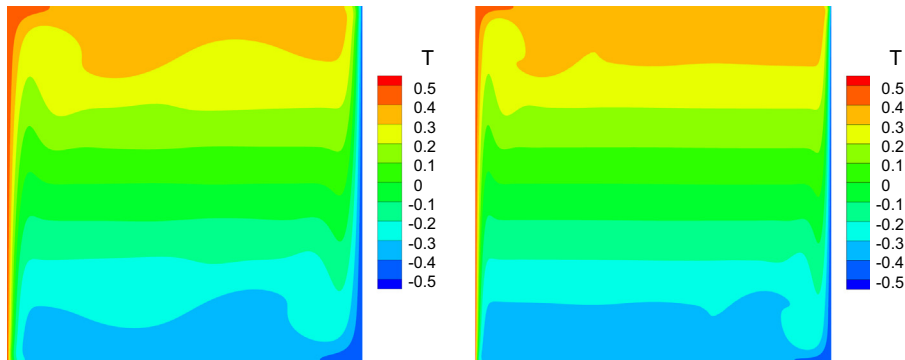
Fig. 2. Temperature field of laminar simulation on computational mesh $80 \times 80R10$: results of steady state simulation at $Ra = 10^7$ (left) and instantaneous results of unsteady simulation at $Ra = 10^8$ (right).
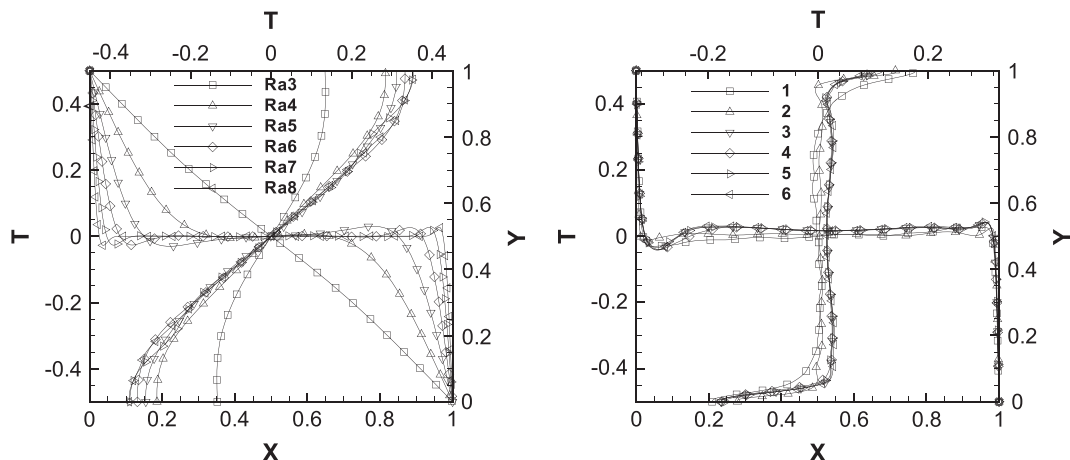
Fig. 3. Temperature profiles of natural convection flow simulation on computational mesh $80 \times 80R10$: laminar steady state simulation for Rayleigh numbers from $Ra = 10^3$ to $Ra = 10^7$ (left), laminar time averaged simulation for $Ra = 10^8$ (left) and simulations using hybrid models 1–6 for Rayleigh number $Ra = 10^9$ (right).
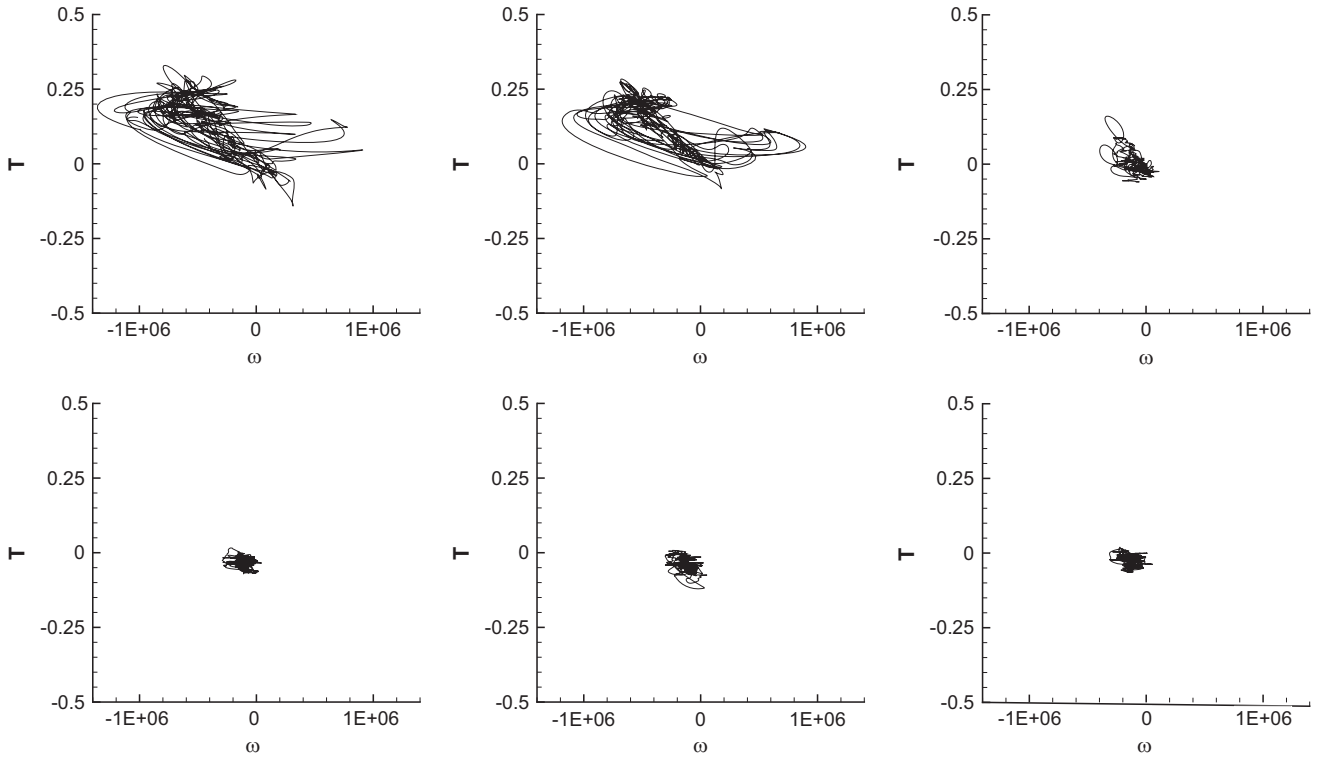
Fig. 4. Temperature T and vorticity ω in point (0.05061, 0.05061) at $Ra = 10^9$ using hybrid model: 1 (top left), 2 (top middle), 3 (top left), 4 (bottom left), 5 (bottom middle) and 6 (bottom right).
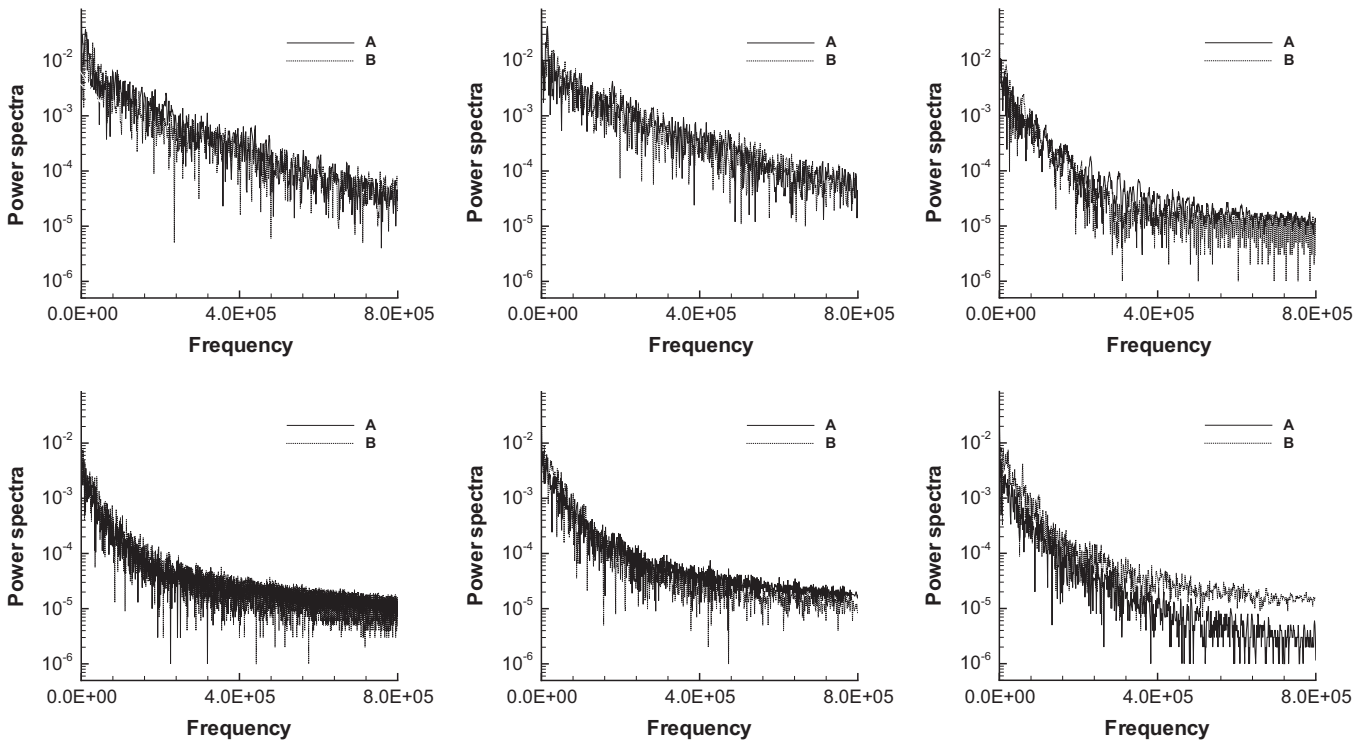
Fig. 5. Power spectra of temperature time series at point A (0.05061, 0.05061) and B (0.09857, 0.09857) using hybrid models: 1 (top left), 2 (top middle), 3 (top left), 4 (bottom left), 5 (bottom middle) and 6 (bottom right).

whether the impact is due to lower turbulent viscosity or lower heat conductivity within URANS region.

For $Ra = 10^9$ the value of switching criterion was $C_{switch} = 30$ for hybrid models 1 and 2, and $C_{switch} = 60$ for hybrid models 3–6. Fig. 8 shows LES and URANS zones of hybrid model in natural

convection simulation at $Ra = 10^9$. Graphs in Fig. 9 show a ratio of the LES region area according to the whole simulation area. It can be seen from Figs. 8 and 9 that models with switching criterion Re_{tot} 3–6 have more dynamic interfaces than models 1 and 2, where Re_k is used for switching criterion. The difference in
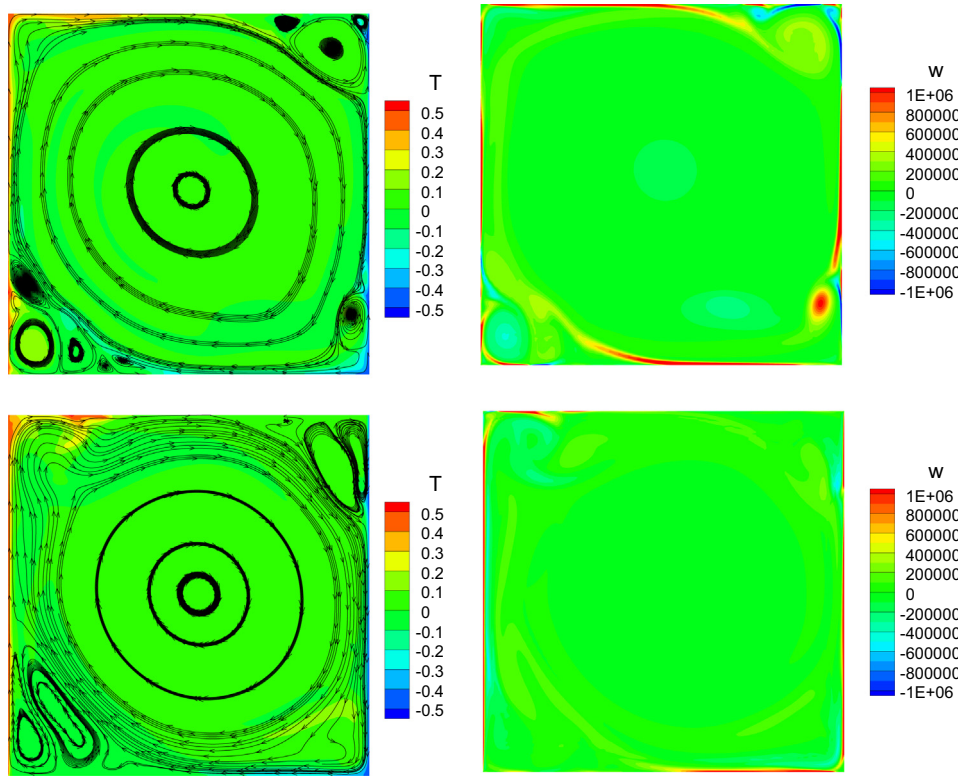
Fig. 6. Temperature (left) and vorticity (right) field at $Ra = 10^9$ using hybrid model 1 in time step 13843 (top) and hybrid model 3 in time step 29719 (bottom).
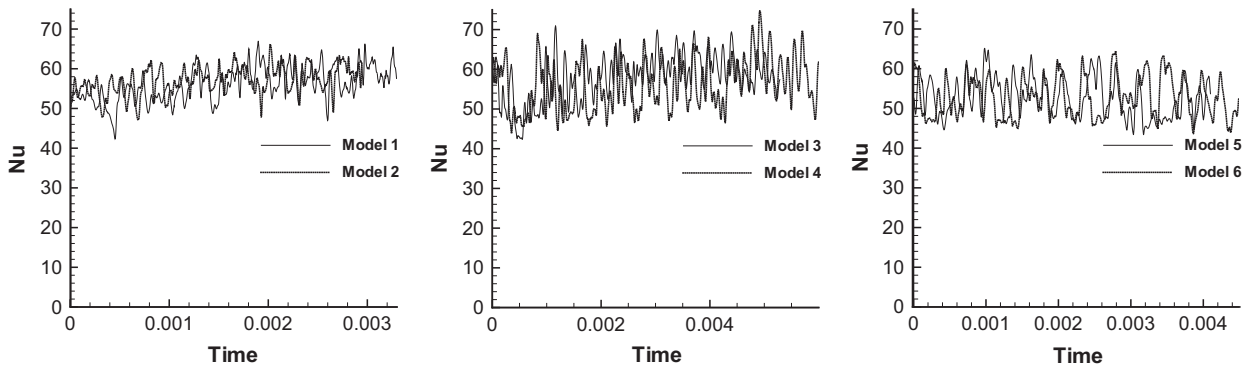
Fig. 7. Nusselt number for Rayleigh number $Ra = 10^9$ using computational mesh $80 \times 80R10$. In the left of the figure are results for hybrid model 1 (—–) and hybrid model 2 (⋯⋯), in the middle figure for hybrid model 3 (—–) and hybrid model 4 (⋯⋯) and in the right figure for hybrid model 5 (—–), and hybrid model 6 (⋯⋯).

Table 3

Nusselt numbers for natural convection flow simulation using different turbulent LES/URANS hybrid models.

Hybrid model	1	2	3	4	5	6	Barakos et al. [1]	Dixit and Babu [6]
$Ra = 10^9$	56.0	56.5	57.7	56.2	52.6	52.9	(54.4) 60.1	57.35

interface dynamics occurs when defining the quantity used for the switching criterion. Although Re_k is a dynamic quantity, it only depends on the current modelled turbulent kinetic energy k. Re_{tot} depends on the current modelled turbulent kinetic energy k and on the difference between the averaged and current solved velocity fields. The graph in Fig. 7 (left) shows the Nusselt number for $Ra = 10^9$ for all hybrid models. It can be seen that the smallest amplitude of the Nusselt number is by using hybrid models 1 and

2, and the biggest using hybrid model 4. The results obtained using hybrid models 1 and 2 are damper in comparison with the results obtained using models 3–6.

The averaged Nusselt number results for $Ra = 10^9$ are summarized in Table 3 and compared with the results from other researchers. Barakos et al. [1] used DNS and two-equation URANS model $k-\epsilon$ for natural convection flow simulation, averaged Nusselt numbers for $Ra = 10^9$ were 54.4 using DNS and 60.1 using $k-\epsilon$. Dixit and Babu [6] used the lattice Boltzmann method, averaged Nusselt number for $Ra = 10^9$ was 57.35. It can be seen from averaged Nusselt number, that the results obtained with the LES/URANS hybrid model are within same range. From graphs with Nusselt number 7 and from the averaged Nusselt number data (Table 3) it can be seen that different URANS models, switching criteria and the use of a modification function do affect the simulation results. URANS islands did not adversely impact on hybrid models 1 and 2, where the Reynolds number based on turbulent kinetic energy Re_k is used as the switching
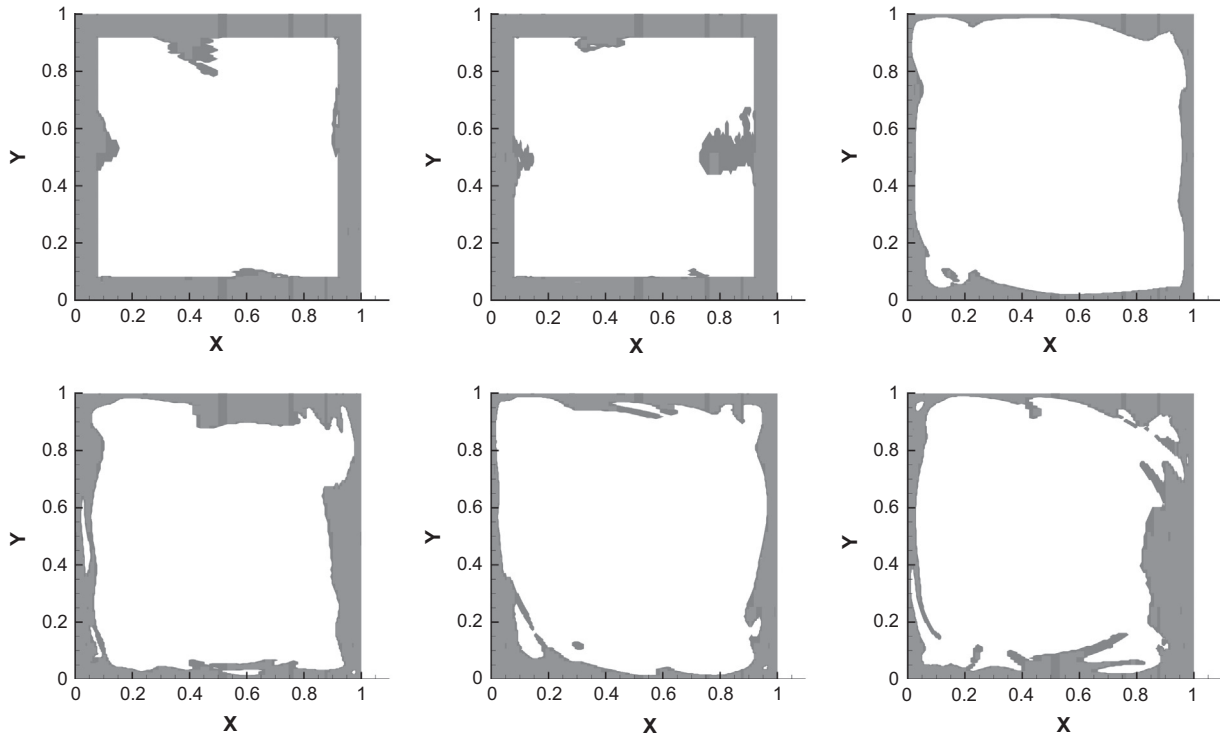
Fig. 8. LES (white) and URANS (grey) zones in natural convection simulation for Rayleigh number $Ra = 10^9$ using computational mesh $80 \times 80R10$ and LES/URANS turbulent hybrid model: 1 (top left), 2 (top middle), 3 (top right), 4 (bottom left), 5 (bottom middle), and 6 (bottom right).
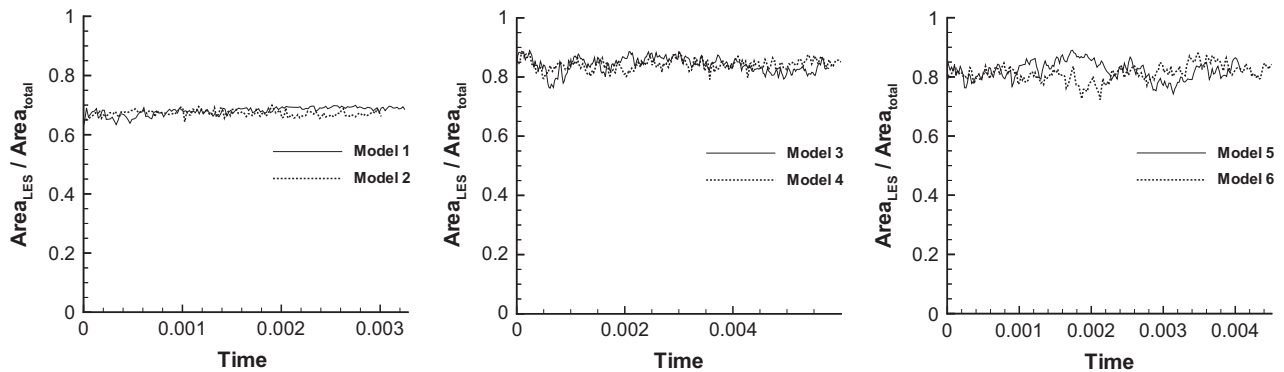
Fig. 9. Ratio of LES region area according to the whole simulation area for hybrid models: 1 and 2 (left), 3 and 4 (middle) and 5 and 6 (left).

criteria. On the other hand, URANS islands do have a slight impact on simulations using hybrid models where the Reynolds number based on total turbulent kinetic energy Re_{tot} was used, that means hybrid models 3–6. URANS islands do not affect the temperature field directly, but they do affect the turbulent quantities, turbulent viscosity ν_t and turbulent heat conductivity a_t. Because ν_t and a_t are being further used in turbulent kinetic energy k transport equation computation and fluid flow computation, it significantly affects convergence.

8. Conclusions

The developed LES/URANS hybrid turbulent model was, in combination with BEM based algorithm and velocity–vorticity formulation of governing equations, successfully used for solving unsteady non-isothermal turbulent phenomena. The numerical algorithm was tested using natural convection flow within a square cavity. We used a direct simulation for Rayleigh numbers up to $Ra = 10^8$. Fluid flow up to $Ra = 10^7$ is steady, at $Ra = 10^8$ the flow becomes unsteady, but still

periodic and non-chaotic. Transition to turbulent flow occurs between $Ra = 10^8$ and 10^9. It can be seen from the temperature and vorticity field, and the vorticity–temperature phase diagrams, that flow becomes unsteady and chaotic. A unified one-equation LES/URANS hybrid turbulent model, that is based on transport equation for turbulent kinetic energy k, was used for developed turbulent flow. The interface between LES and URANS is defined dynamically during simulation. For switching criterion we employed the Reynolds number based on turbulent kinetic energy Re_k and the Reynolds number based on total kinetic energy Re_{tot}. In further simulations, we used a modification function for the URANS region. The results obtained with the LES/URANS hybrid model for $Ra = 10^9$ are in good agreement with the results from Barakos et al. [1] and results from Dixit and Babu [6].

References

[1] Barakos G, Mitsoulis E, Assimacopoulos D. Natural convection flow in a square cavity revisited: laminar and turbulent models with wall function. Int J Numer Methods Fluids 1994;18:695–719.

[2] Breuer M, Jaffrezic B, Arora K. Hybrid LES/RANS technique based on a one-equation near-wall model. Theor Comput Fluid Dyn 2008;22:157–87.

[3] Davidson L. The {PANS} model in a zonal hybrid RANS-LES formulation. Int J Heat Fluid Flow 2014;46:112–26.

[4] Davidson L, Billson M. Hybrid LES-RANS using synthesized turbulent fluctuations for forcing in the interface region. Int J Heat Fluid Flow 2006;27 (6):1028–42.

[5] Davies GDV. Natural convection of air in a square cavity: a bench mark numerical solution. Int J Numer Methods Fluids 1983;3:249–64.

[6] Dixit HN, Babu V. Simulation of high Rayleigh number natural convection in a square cavity using the lattice Boltzmann method. Int J Heat Mass Transf 2006;49:727–39.

[7] Froehlich J, Terzi Dv. Hybrid LES/RANS methods for the simulation of turbulent flows. Prog Aerosp Sci 2008;44(5):349–77.

[8] Jenny Patrick, Xiao Heng. A consistent dual-mesh framework for hybrid LES/RANS modeling. J Comput Phys 2012;231:1848–65.

[9] Jaffrézic B, Breuer M. Application of an explicit algebraic reynolds stress model within a hybrid LES/RANS method. Flow Turbul Combust 2008;81:415–48.

[10] Kenjereš S, Hanjalič K. LES, T-RANS and hybrid simulations of thermal convection at high Ra numbers. Int J Heat Fluid Flow 2006;27(5):800–10.

[11] Lo DC, Young DL, Murugesan K, Tsai CC, Gou MH. Velocity–vorticity formulation for 3D natural convection in an inclined cavity by DQ method. Int J Heat Mass Transf 2007;50:479–91.

[12] Lupše J, Škerget L, Ravnik J. Velocity–vorticity {RANS} turbulence modeling by boundary element method. Eng Anal Bound Elem 2014;39:44–52.

[13] Moser RD, Kim J, Mansour NN. Direct numerical simulation of turbulent channel flow up to $Re_\tau = 590$. Phys Fluids 1999;11:943–5.

[14] Paik J, Sotiropoulos F, Porté-Agel F. Detached eddy simulation of flow around two wall-mounted cubes in tandem. Int J Heat Fluid Flow 2009;30 (2):286–305.

[15] Pope SB. Turbulent flows. Cambridge, United Kingdom: Cambridge University Press; 2000.

[16] Quéméré P, Sagaut P. Zonal multi-domain RANS/LES simulations of turbulent flows. Int J Numer Methods Fluids 2002;40(7):903–25.

[17] Ramšak M, Škerget L. Boundary element method for thermal flows using $k–\epsilon$ turbulence models. Numer Methods Heat Fluid Flow 2008;18(3–4):514–32.

[18] Ravnik J, Škerget L, Hriberšek M. 2D velocity vorticity based LES for the solution of natural convection in a differentially heated enclosure by wavelet transform based BEM and FEM. Eng Anal Bound Elem 2006;30:671–86.

[19] Rodi W, Mansour NN, Michelassi V. One-equation near-wall turbulence modeling with the aid of direct simulation data. ASME Trans, J Fluids Eng 1993;115:196–205 (ISSN 0098-2202).

[20] Sajjadi H, Gorji M, Hosseinizadeh SF, Kefayati GR, Ganji DD. Numerical analysis of turbulent natural convection in Square cavity using large-eddy simulation in lattice Boltzmann method. Trans Mech Eng 2011:133–42.

[21] Samec N, Škerget L. Integral formulation of a diffusive–convective transport equation for reacting flows. Eng Anal Bound Elem 2004;28(9):1055–60.

[22] Schmidt S, Breuer M. Hybrid LES-URANS methodology for the prediction of non-equilibrium wall-bounded internal and external flows. Comput Fluids 2014;96:226–52.

[23] Schumann U. Subgrid scale model for finite difference simulations of turbulent flows in plane channels and annuli. J Comput Phys 1975;18(August (4)):376–404.

[24] Sleijpen GLG, Fokkema DR. BiCGstab (l) for linear equations involving unsymmetric matrices with complex spectrum. Electron Trans Numer Anal 1993;1:11.

[25] Spalart PR, Shur M. On the sensitization of turbulence models to rotation and curvature. Aerosp Sci Technol 1997;1(5):297–302.

[26] Škerget L, Hriberšek M, Žunic Z. Natural convection flows in complex cavities by BEM. Int J Numer Methods Heat Fluid Flow 2003;13:720–35.

[27] Škerget L, Rek Z. Boundary-domain integral method using a velocity-vorticity formulation. Eng Anal Bound Elem 1995;15:359–70.

[28] Tessicini F, Temmerman L, Leschziner MA. Approximate near-wall treatments based on zonal and hybrid RANS-LES methods for LES at high Reynolds numbers. Int J Heat Fluid Flow 2006;27(5):789–99.

[29] Warsi ZUA. Fluid dynamics, theoretical and computational approaches. Boca Raton, Florida, USA: CRC Press; 1993.